Solid Earth, 12, 237–251, 2021
https://doi.org/10.5194/se-12-237-2021

Solid Earth Open Access EGU

Extensional reactivation of the Penninic frontal thrust 3 Myr ago as evidenced by U–Pb dating on calcite in fault zone cataclasite

Antonin Bilau[1,2], Yann Rolland[1,2], Stéphane Schwartz[2], Nicolas Godeau[3], Abel Guihou[3], Pierre Deschamps[3], Benjamin Brigaud[4], Aurélie Noret[4], Thierry Dumont[2], and Cécile Gautheron[4]

[1]EDYTEM, Université Savoie Mont Blanc, CNRS, UMR 5204, 73370 Le Bourget-du-Lac, France
[2]ISTerre, Université Grenoble Alpes, Univ. Savoie Mont Blanc, CNRS, IRD, IFSTTAR, 38000 Grenoble, France
[3]Aix-Marseille Université, CNRS, IRD, INRAE, Collège de France, CEREGE, 13545 Aix-en-Provence, France
[4]GEOPS, CNRS, Université Paris-Saclay, 91405 Orsay, France

Correspondence: Antonin Bilau (antonin.bilau@univ-smb.fr) and Yann Rolland (yann.rolland@univ-smb.fr)

Received: 10 July 2020 – Discussion started: 2 September 2020
Revised: 8 December 2020 – Accepted: 11 December 2020 – Published: 28 January 2021

Abstract. In the Western Alps, the Penninic frontal thrust (PFT) is the main crustal-scale tectonic structure of the belt. This thrust transported the high-pressure metamorphosed internal units over the non-metamorphosed European margin during the Oligocene (34–29 Ma). Following the propagation of the compression toward the European foreland, the PFT was later reactivated as an extensional detachment associated with the development of the High Durance extensional fault system (HDFS). This inversion of tectonic displacement along a major tectonic structure has been widely emphasized as an example of extensional collapse of a thickened collisional orogen. However, the inception age of the extensional inversion remains unconstrained. Here, for the first time, we provide chronological constraints on the extensional motion of an exhumed zone of the PFT by applying U–Pb dating on secondary calcites from a fault zone cataclasite. The calcite cement and veins of the cataclasite formed after the main fault slip event, at 3.6 ± 0.4–3.4 ± 0.6 Ma. Cross-cutting calcite veins featuring the last fault activity are dated at 2.6 ± 0.3–2.3 ± 0.3 Ma. $\delta^{13}C$ and $\delta^{18}O$ fluid signatures derived from these secondary calcites suggest fluid percolation from deep-seated reservoir at the scale of the Western Alps. Our data provide evidence that the PFT extensional reactivation initiated at least ~ 3.5 Myr ago with a reactivation phase at ~ 2.5 Ma. This reactivation may result from the westward propagation of the compressional deformation toward the external Alps, combined with the exhumation of external crystalline massifs. In this context, the exhumation of the dated normal faults is linked to the eastward translation of the HDFS seismogenic zone, in agreement with the present-day seismic activity.

1 Introduction

Dating of major tectonic inversions in orogens is generally achieved by indirect and relative dating, but rarely by the direct dating of fault-related minerals using absolute geochronometers. For instance, tectonic cycles are defined worldwide by the sediment unconformities or by exhumation ages through thermochronological investigation. However, the recent progress in U–Pb dating of carbonate using high-resolution laser ablation analyses (Roberts et al., 2020) allows us to directly date minerals formed during fault activity and thus to establish the age of tectonic phases by absolute radiometric dates (Ring and Gerdes, 2016; Goodfellow et al., 2017; Beaudoin et al., 2018). This method is especially well suited to disentangle the successive tectonic motions along a given tectonic structure. U–Pb dating can be coupled to stable isotopic analysis to infer the nature of fluids through time, which may give insights into the scale of fluid circulations and thus the scale of the active tectonic structure and changes in the stress regime (e.g. Beaudoin et al., 2015; Rossi and Rolland, 2014). In the Western Alps, the Penninic frontal thrust, or PFT, represents a major thrust structure at lithospheric scale (e.g. Tardy et al., 1990; Mugnier et al., 1993; Zhao et al., 2015) that accommodated the main collisional phase during the Palaeogene–Neogene (e.g.

Ceriani et al., 2001; Ceriani and Schmid, 2004). Later on, this thrust was reactivated as a normal fault, and the extensional deformation is still ongoing (Sue and Tricart, 1999; Tricart et al., 2006; Sue et al., 2007). This transition from compression to extension in a collisional chain has been diversely interpreted to reflect slab break-off, crustal overcompensation or post-glacial and erosion-induced isostatic rebound (e.g. Champagnac et al., 2007; Sternai et al., 2019). However, until now, no direct dating of the tectonic shift from compression to extension on the PFT has been obtained, which leads to many possible geodynamic scenarios. At the present day, a large range of ages for this transition have been hypothesized, from ∼ 12–5 Ma (Tricart et al., 2006) to only a few tens of thousands of years (Larroque et al., 2009), which shows the lack of direct dating of brittle deformation (Bertrand and Sue, 2017). In this study, we applied the laser ablation U–Pb dating method on secondary calcites from a cataclasite fault zone that testify to the extensional deformation of an exhumed palaeo-normal fault during the PFT inversion.

The purpose of this study is (1) to provide absolute chronological constraints on the structural inversion of the PFT and (2) to give insights into the scale and nature of fluid circulations along this major fault using stable isotope analysis of carbon and oxygen.

2 Geological setting

The western Alpine collisional belt results from the convergence and collision of the European and Apulian plates, which culminated with top-to-the-west displacement on the PFT acting as the major Alpine tectonic structure in the Late Eocene to Oligocene times (e.g. Dumont et al., 2012; Bellahsen et al., 2014). This lithospheric-scale structure accommodated westward thrusting of highly metamorphosed "internal zone" units over slightly metamorphosed "external zone" units (Fig. 1; Schmid and Kissling 2000; Lardeaux et al., 2006; Simon-Labric et al., 2009; Malusà et al., 2017). The external zone is composed of the non-metamorphosed European Mesozoic and Palaeozoic sedimentary cover and its Palaeozoic basement corresponding to the external crystalline massifs (ECMs).

The internal zone corresponds to a high-pressure metamorphic wedge formed by the stacking of the palaeo-distal European margin of the Briançonnais zone, comprising the internal crystalline massifs and their sedimentary cover, with the oceanic-derived units of the Piedmont zone. These units were incorporated and juxtaposed in the subduction accretionary prism from the early Late Cretaceous until the late Eocene (e.g. Agard et al., 2002; Schwartz et al., 2007). The timing of subduction and collision is well constrained by numerous dates on metamorphic minerals (e.g. Duchêne et al., 1997; Rubatto and Hermann, 2003; Lanari et al., 2012, 2014). Eclogite facies recrystallization records subduction of the distal European margin at 32.8 ± 1.2 Ma in the Dora-Maira massif, which was later transported as a tectonic nappe during the collision (Duchêne et al., 1997). PFT activation and underthrusting of external crystalline massifs are indicators of the transition from subduction to continental collision in the internal zones, between 44 and 36 Ma (e.g. Beltrando et al., 2009). This transition is marked by shear zone development in greenschist facies conditions and recrystallization during burial of the Alpine external zone in the PFT footwall compartment (Rossi et al., 2005; Sanchez et al., 2011; Bellahsen et al., 2014). The early ductile PFT activity is dated at 34–29 Ma by $^{40}Ar/^{39}Ar$ dating of syn-kinematic phengite from shear zones in the Pelvoux and Mont Blanc external crystalline massifs (Seward and Mancktelow, 1994; Rolland et al., 2008; Simon-Labric et al., 2009; Bellanger et al., 2015; Bertrand and Sue, 2017) and by U–Pb on allanite (Cenki-Tok et al., 2014). The age of the PFT hanging wall tectonic motion and joint erosion is highlighted by the exhumation of the Briançonnais units constrained by apatite fission tracks (AFTs) at 26–24 Ma (Tricart, 1984; Tricart et al., 2001, 2007; Ceriani and Schmid, 2004). However, the PFT reactivation as a normal fault remains unconstrained. The onset of PFT extensional activity has been proposed to have occurred in the late Miocene (∼ 12 to 5 Ma), based on indirect AFT ages in the Pelvoux external crystalline massif (Tricart et al., 2001, 2007), which record a cooling episode related to relief creation and erosion. The current seismicity (e.g. Rothé, 1942; Sue et al., 1999, 2007) and observed GPS motions (Walpersdorf et al., 2018; Mathey et al., 2020) all along the so-called High Durance fault system (HDFS) highlight the fact that extensional and minor strike-slip deformations along the PFT are still ongoing. This seismicity mostly occurs at shallow depths, less than 10 km, and mainly at 3 to 8 km, where the HDFS is structurally connected to the PFT (Sue and Tricart, 2003; Thouvenot et al., 2006; Sue et al., 2007).

The study area is focused on a portion of the PFT located in the southeast of the Pelvoux external crystalline massif in the Western Alps (France) (Figs. 1–2). Here, the PFT rests on late Eocene (Priabonian) autochthonous nummulitic flysch, so-called "Champsaur sandstone" (Fig. 2), which lies unconformably on the Pelvoux crystalline basement. In the southern part, the PFT lies on the Cretaceous helminthoid flysch nappes (Fig. 2). These two flysch units are intensely deformed by top-to-the-west PFT compressional deformation. The PFT hanging wall corresponds to the Briançonnais zone composed of Mesozoic and Palaeozoic sedimentary units, which underwent high-pressure metamorphism (Lanari et al., 2012, 2014). The Briançonnais zone is composed of the Briançonnais zone houillère, which consists of Carboniferous sediments overlying a crystalline basement, stratigraphically overlain by Middle Triassic–Cretaceous sediments (limestones and calcschists). The PFT structure is well shown in the Tête d'Oréac section of the Fournel Valley transect (Fig. 3,;Sue and Tricart, 1999). Here, normal faults cross-cut the Briançonnais series and branch down on the PFT, which was reactivated as a detachment (Tricart et al., 2001).

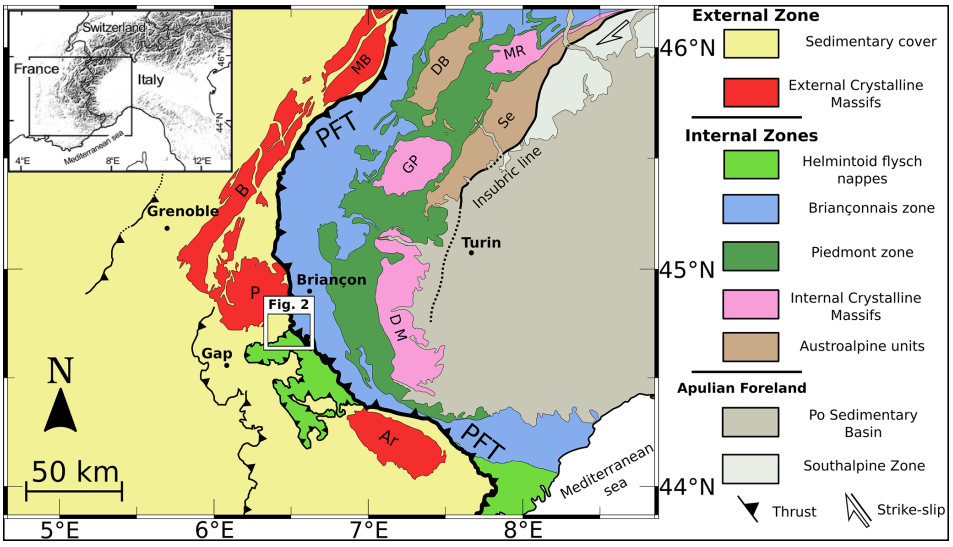

Figure 1. Geological map of the Western Alps showing the location of the study area. External crystalline massifs: Ar, Argentera; B, Belledonne; MB, Mont Blanc; P, Pelvoux. Internal crystalline massifs: DM, Dora-Maira; GP, Grand Paradis; MR, Mont Rose. PFT: Penninic frontal thrust. Insert modified from Schwartz et al. (2017).

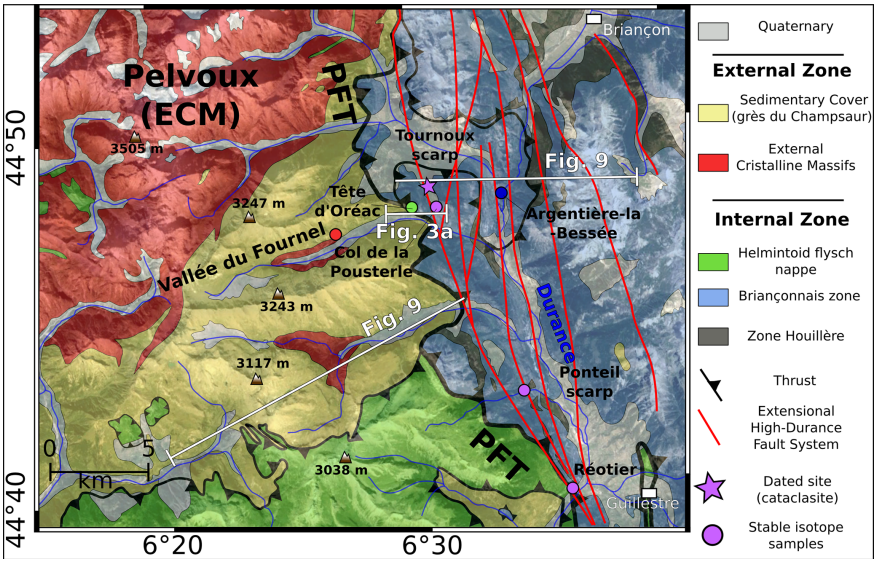

Figure 2. Study area of the Penninic frontal thrust, east of the Pelvoux external crystalline massif (ECM). The High Durance fault system is represented in red from Tricart et al. (2001) and Sue et al. (2007). Location of sampled sites is indicated. The location of the extensional fault dated by U–Pb on calcite (samples FP18-2 and FP18-3) is marked by a star. Colour of site circle refers to the host rock age: red, Eocene sandstone flysch (grès du Champsaur); green, Cretaceous carbonates; blue, Jurassic carbonates; purple, Triassic carbonates. Sample descriptions are shown in Fig. S1. © Google Earth for background relief map.

The normal faults are tilted by a passive rotation of about 30° towards the west during their exhumation in relation to the activity of the High Durance fault system (Sue et al., 2007).

3 Sampling strategy and analytical methods

3.1 Sampling strategy

We collected key samples of each brittle–ductile deformation phase, both in the PFT footwall and hanging wall (Table S1 in the Supplement), to provide a petrographic and stable isotopic dataset which will allow discussing the nature of fluids

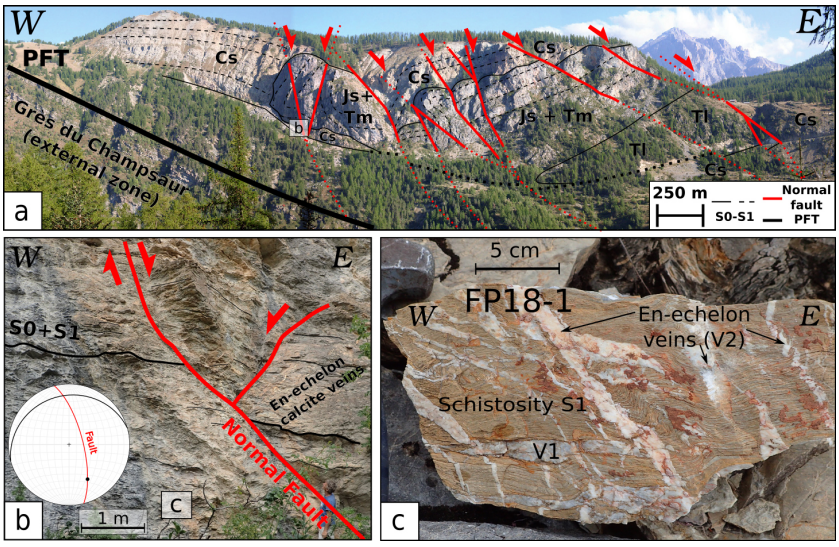

Figure 3. **(a)** General view and geological interpretation of the Fournel Valley southern slope with the studied site of the Tête d'Oréac. **(b)** Outcrop interpretation of the Tête d'Oréac with extensional features in Late Cretaceous calcschists in agreement with the High Durance fault system and Wulff stereogram, lower hemisphere. **(c)** Calcschist-oriented sample FP18-1 evidencing multiple calcite vein generations. V1 is related to the main compressional phase related to the Tête d'Oréac anticline formation, and V2 are related to extensional reactivation of the PFT during onset of the High Durance fault system. Cs: Late Cretaceous calcschists; Js + Tm: Middle Triassic–Late Jurassic dolomitic–siliceous limestones; Tl: Lower Triassic sandstones.

throughout the PFT activity associated with the late compressional and extensional history. Field analysis is supported by petrographic observations of 28 samples, including 8 host rocks, 6 from compressional structures and 14 from extensional structures. Based on this dataset, we selected three fault breccia samples with which to date the PFT extensional reactivation.

3.2 Cathodoluminescence

Cathodoluminescence (CL) analysis provides shades that are mainly representative of the oxidation state of a trace element and their contents, i.e. Mn^{2+} and Fe^{2+} (Barnaby and Rimstidt, 1989). These differences in calcite chemical composition are an indicator of different mineral precipitations related to slight variations in fluid composition (Goodfellow et al., 2017). CL can also highlight crystal growth patterns or grain boundary interactions (Beaudoin et al., 2015). Using cross-cutting criteria as well as CL, a relative chronology of the calcite generations and related microstructures has been made. Analyses were performed with a spot-camera-mounted cathodyne device (cold cathode) with the following parameters: ∼ 50 mTorr vacuum, 16–18 kV voltage and ∼ 200 µA electron beam. The description terminology used is based on Bons et al. (2012).

3.3 O and C stable isotope analysis

Stable isotope measurements were achieved for the different generations of microstructures identified by thin-section observations and CL images, at Geosciences Paris Sud (GEOPS) laboratory of the Paris-Saclay University, France. Results are presented in Table 1. The protocol is described in detail by Andrieu et al. (2015). Several milligrams (∼ 1 mm^3) of sample for each calcite generation were collected using a Dremel 4000 with a 3.2 mm head. Samples were then dissolved with pure orthophosphoric acid (H_3PO_4): sample tubes provided with two compartments (one for the sample and one for the acid) were sealed under a pressure of 1.5×10^{-2} mbar. They were immersed in a water bath at 25 °C before the acid was poured on the sample and left to react for 24 h. Complete reaction is necessary to avoid any artificial isotopic fractionation. The produced CO_2 is collected using an extraction line, and a liquid nitrogen trap is used to ensure that only CO_2 is collected. Pure CO_2 is analysed on a VG SIRA 10 dual-inlet isotope ratio mass spectrometer. Data validity is supported by concurrent analysis of the international standard IAEA CO-1. $\delta^{13}C$ and $\delta^{18}O$ are expressed per mil relative to V-PDB (Vienna Pee Dee Belemnite) by assigning a $\delta^{13}C$ value of +1.95 ‰ and a $\delta^{18}O$ value of −2.20 ‰ to NBS19 (Eq. 1).

$$\delta^{13}C = \left[\frac{\left(^{13}C/^{12}C\right)_{Sample}}{\left(^{13}C/^{12}C\right)_{Reference}} - 1 \right] \times 1000 \quad (1)$$

For oxygen isotope measurements, a switch from PDB values to SMOW (standard mean oceanic water) was made using the Kim et al. (2015) equation (Eq. 2).

$$\delta^{18}O_{SMOW} = 1.03086 \times \delta^{18}O_{PDB} + 30.86 \quad (2)$$

Table 1. Isotopic composition of analysed calcites. Stable isotope data from host rocks, calcite veins and cataclasite fillings of extensional faults.

	Number of sample	$^{13}\delta$C PDB	$^{18}\delta$O SMOW
Host rock	FP18-1A	2.15	17.18
	FP18-1A	2.09	16.90
	FP18-4	1.92	24.83
	FP18-7	2.25	25.76
	FP18-9	−0.32	22.00
	FP18-10	1.26	28.59
	FP18-11	2.1	26.51
	FP18-13	3.43	23.73
Early veins (V1)	FP18-1B	2.59	19.89
	FP18-1C	2.48	20.74
	FP18-1C	2.48	18.84
	FP18-9	−0.18	22.59
	FP18-10	1.29	28.99
	FP18-11	1.58	23.37
En-echelon veins (V2)	FP18-1A	2.12	17.65
	FP18-1A	2.18	18.15
	FP18-1B	1.96	17.71
	FP18-1D	1.88	17.98
	FP18-5	1.66	25.80
Cataclasite infill (V2)	FP18-2A	0.03	7.43
	FP18-2B	−0.09	7.86
	FP18-3B	−4.62	11.41
	FP18-3B	−0.75	12.10
	FP18-6	−3.04	10.23
	FP18-6	−0.95	12.68
	FP18-13	3.46	13.29
	FP18-13	2.53	14.38
	FP18-13	3.4	7.21

The ratio of carbon to oxygen isotopes is related to the parental fluid of calcite and can be used as a fluid tracer. Reproducibility was checked by replicate analysis of in-house standards and was ±0.2 ‰ for oxygen isotopes and ±0.1 ‰ for carbon isotopes.

3.4 U–Pb dating of calcite

In situ uranium and lead isotope analyses of carbonates were carried out at CEREGE (Centre Européen de Recherche et d'Enseignement des Géosciences de l'Environnement), Aix-en-Provence, France. Results are presented in Table S2. Data were acquired on 150 µm thick thin sections. Laser ablation analysis was performed with an ESI excimer laser ablation system with a 6 in. (1.524×10^{-1} m) two-volume cell (ESI), coupled to an Element XR SF-ICP-MS (sector field inductively coupled mass spectrometer, Thermo Fisher Scientific). Analyses were done at 10 Hz and 1.1–1.15 J cm^{-2}. Samples were first screened to check signal intensities and maximize the spread of ^{238}U/^{206}Pb ratios (e.g. map of Fig. S3 in the Supplement) to obtain the highest U–Pb variability. A typical analysis consists of 3 s of preablation to clean the sample surface, followed by 20 s of gas blank and ∼ 20 s of measurement on a static circle spot of 150 µm diameter (approximately eight to nine acquisition cycles per second). These parameters lead to an approximately ∼ 20–25 µm deep hole (∼ 1 µm s^{-1}) on a carbonate material. Ablated particles are carried out of the cell with a He gas flux of 1300 mL min^{-1} and then mixed with Ar sample gas (typically 0.8–0.9 L min^{-1}). Unknown samples were corrected by standard bracketing with synthetic NIST-614 glass for instrumental drift and lead isotope composition (Woodhead and Hergt, 2001) and a natural calcite spar WC-1 of 254.4 ± 6.4 Ma (Roberts et al., 2020) for inter-elemental fractionation effect, every 20 measurements. No downhole correction was applied since no natural calcite standard with a homogeneous U / Pb ratio allows such correction. However, the large aspect ratio used in this set-up is supposed to limit this effect. Unknown samples were first processed with Iolite software (Paton et al., 2011) for baseline correction. Raw ratios were then reduced for instrumental drift, lead isotope composition and inter-elemental fractionation using an in-house excel spreadsheet macro designed for carbonate samples. Ages are obtained using IsoplotR software and plotted on a Tera-Wasserburg diagram using model (1) age (Vermeesch, 2018). An additional error propagation of 2.51 % in quadratic addition on the final age, tied to the WC-1 standard, is expressed in brackets on the Tera-Wasserburg plot.

4 Results

4.1 Deformation phases and microstructures

4.1.1 Brittle–ductile deformation features

During the westward thrust motion of the PFT, the Tête d'Oréac cross section passes through the PFT (Fig. 3) and preserves a succession of units that were stacked on each other. The main schistosity (S1) is parallel to the initial bedding (S0) in Cretaceous calcschists. S0–S1 is sub-horizontal and penetrative throughout the studied area. At the outcrop scale, S1 is clearly visible and shows a dissolution surface with the development of stylolithic joints (Fig. 4).

Quartz anisotropy is observable in LPA, which indicates an important deformation syn- to post-V1 formation. This suggests a strong transposition of structures during PFT compressional motion or that the veins opened initially in an orientation parallel to S1; either way a ductile deformation is recorded. These early shortening features are cross-cut by numerous steeply dipping eastward normal faults linked to the extensional reactivation of PFT. Early stages of extension are featured by centimetre-scale "en-echelon" veins (V2) indicative of an early brittle–ductile extensional deformation

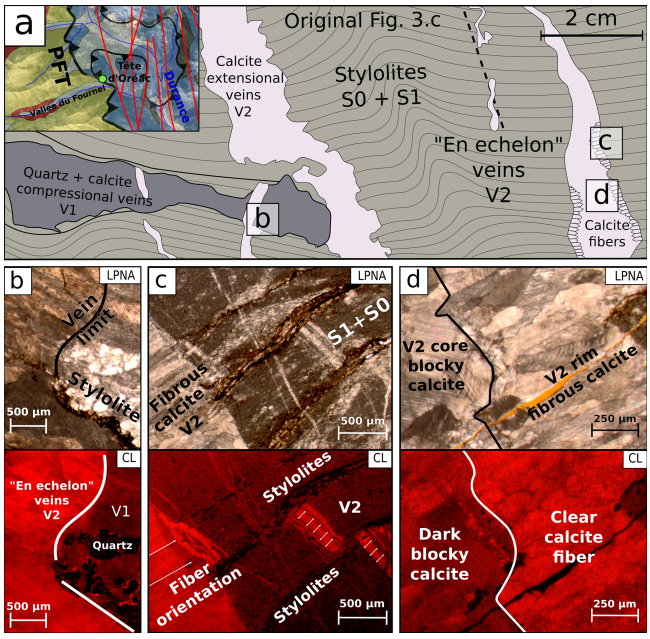

Figure 4. **(a)** General sketch of sample FP18-1 evidencing cross-cutting relationships for two main vein generations (Fig. 3c). **(b–d)** Microscope and cathodoluminescence pictures showing the different vein calcite generations.

followed by dissolution on the horizontal composite (S0–S1) cleavage. Larger V2 veins, expressed at centimetre scale, cross-cut the cleavage and show elongated calcite fibres of $\sim 1000\,\mu m$ at the vein walls (Fig. 4). Similar shades for early V2 and fibrous V2 are observed in CL. At vein cores, the fibrous calcite is then replaced by a blocky calcite that is less luminescent in CL.

4.1.2 Brittle deformation features

The internal structure of one major extensional fault is investigated in the Tournoux scarp (Fig. 5). The fault zone is highlighted by a metre-scale cataclasite fault gouge with variable amounts of deformations. The top-to-the-east (N90° E) normal sense of shear is represented by sigmoids and down-dip slickenside. At thin-section scale, for sample FP18-2, the cataclasite is composed of centimetre-scale host rock clasts with very small ($< 20\,\mu m$) limestone grains. Two types of calcite fillings have been identified. The first one contains organic matter and has a "dusty appearance" with bright shades in CL (Fig. 5c). The second one shows large and clear crystals that grew in the cracks and porosity, showing sector zoning patterns highlighted in CL and laser ablation inductively coupled plasma mass spectrometry (LA-ICP-MS) maps (Figs. 5d and S3). Approximately 700 µm large clear, hexagonal and organic-matter-free calcite crystals have been selected for U–Pb dating.

These calcite crystals represent the latest pervasive fluid circulation episode through the porosity and provide a minimum age for the cataclasite. In sample FP18-3, the matrix is cross-cut by calcite veins with variable diameters (300–1300 µm) and is free of any further deformation. On the basis of their homogeneity and their youngest relative age relationships, these late calcites have also been targeted for U–Pb calcite dating (see Sect. 4.3). Samples FP19-12A-B (described in the Supplement) were collected in a west-dipping conjugate normal fault and exhibit similar deformation features.

4.2 $\delta^{13}C$ and $\delta^{18}O$ stable isotope results

Stable isotope analyses were performed in calcites from various host rocks samples belonging to the different units highlighted in the studied PFT section (Fig. 3) and are supposed to be representative of the different (compressional and extensional) key tectonic phases (Fig. 6).

For host rock analysis, upper Cretaceous planktonic calcschists from the Tête d'Oréac show the lowest $\delta^{18}O$ host rock value of 16.8–17.1 ‰ and $\delta^{13}C$ of 2.1–2.2 ‰. Triassic carbonates show a range between 23.7 and 26.5 ‰ for $\delta^{18}O$ and between 1.9 and 2.3 ‰ for $\delta^{13}C$ (with a higher value of 3.4 ‰ for the Ponteil scarp). Upper Jurassic calcschists gave a $\delta^{18}O$ ratio of 28.5 ‰ and $\delta^{13}C$ of 1.3 ‰. The western late Eocene flysch (Champsaur sandstone) gave a lowest $\delta^{13}C$ ratio of −0.3 ‰ and a $\delta^{18}O$ ratio of 21.9 ‰. Analysed brittle–ductile veins related either to the compressional phase or to the onset of the extensional tectonic phase stand very close to their host rocks, near to the meteoric water field defined by Nardini et al. (2019) (Fig. 6). However, the V2 veins associated with the brittle normal fault development clearly show lower $\delta^{18}O$ values (< 15 ‰) compared to their host rocks, with a trend towards lower $\delta^{13}C$ values. These isotope signatures are similar to those measured in calcite from veins of the Mont Blanc external crystalline massifs (Rossi and Rolland, 2014).

4.3 Calcite LA-ICP-MS U–Pb dating results

Petrographic analysis has been complemented by screening using LA-ICP-MS on 24 thin sections from samples of 7 locations around the PFT related to shortening and extensional structures. Among these, 20 screened samples show high common lead contents, and sometimes higher lead-to-uranium intensity signals. U–Pb dating of such carbonates with high lead concentrations remains highly challenging, especially for very young samples. However, four samples (samples FP18-2, FP18-3, FP19-12A and FP19B, described in Sect. 4.1 and the Supplement) from the Tournoux normal fault site bear sufficient ^{238}U ($\sim$ 0–8.5 ppm for FP18-3A and FP19-3B, and $\sim$ 0–4.5 ppm for FP18-2B, FP19-12A and FP19-12B), and ^{206}Pb, ^{207}Pb ($\sim$ 0–1.9 ppm for FP18-3A and FP18-3B, and $\sim$ 0–13.1 ppm for FP18-2B, FP19-12A and FP19-12B).

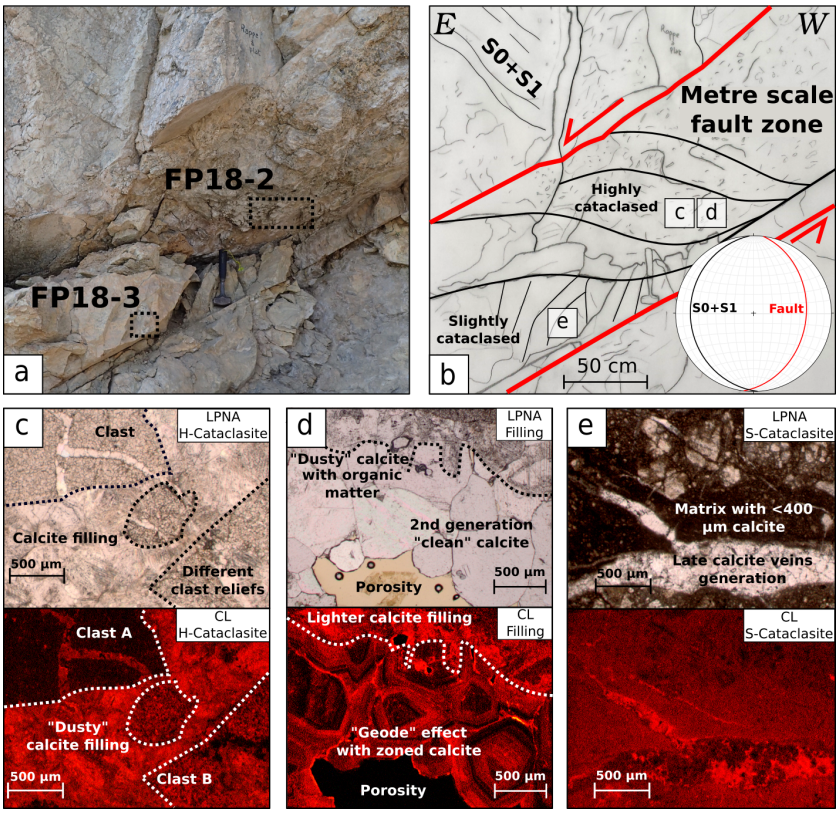

Figure 5. (a–b) Outcrop interpretation of the Tournoux scarp showing various degrees of cataclasis in Triassic dolomitic limestone with Wulff stereogram, lower hemisphere. Squares are sampled area; sample FP18-2 is a highly cataclased sample, while sample FP18-3 is less intensely cataclased and is cross-cut by millimetre-scale calcite veins. **(c–e)** Microscope and cathodoluminescence pictures showing several calcite filling generations. "Clear calcite" shows zonings and seems to crystallize into a primary porosity left within the cataclasite. The clear calcite and veins from the cataclasite are dated using the method of U–Pb dating on calcite.

Lead contents are based on NIST614 intensities, and uranium contents are based on WC-1 intensities (Jochum et al., 2011; Roberts et al., 2017; Woodhead and Hergt, 2001), giving a measurable and significant radiogenic signal. Five ages have been obtained on these four samples (Fig. 7).

A first group of ages of ~ 3.5 Ma is represented by three samples. The cataclasite "clean calcite" infill (sample FP18-2B; Fig. 5) gives an age of 3.42 ± 1.44 Ma ($n = 41$, mean square weighted deviation (MSWD) $= 0.93$). This quite large uncertainty is due to a relatively moderate U / P variability and the resulting low radiogenic signal measurable in this sample. Samples FP19-12A and FP19-12B give two similar within-error ages for the vein calcite and "clean calcite" infill, of 3.55 ± 0.38 ($n = 58$, MSWD $= 1.5$) and 3.43 ± 0.57 ($n = 53$, MSWD $= 0.83$), respectively.

A second group of ages of ~ 2.5 Ma are obtained on different cross-cutting veins of the latest generation of sample FP18-3 (Fig. 5), represented by slightly younger ages, which however are distinctly out of error margins, of 2.59 ± 0.23 Ma ($n = 42$, MSWD $= 1.2$; FP18-3B in Fig. 7b) and 2.34 ± 0.19 Ma ($n = 53$, MSWD $= 1.1$; FP18-3B in Fig. 7c). The higher spread in U / P ratios measured in these two latter ages results in more precise and robust ages. These two age groups obtained on extensional faults connected to the PFT highlight for the first time at least two phases of deformation constrained out of error bars: a first phase of brittle deformation forming the cataclasite at 3.5 ± 0.4 and one or two discrete brittle events at, or within, 2.6 ± 0.2 and 2.3 ± 0.2 Ma. These ages show that the sated conjugated faults have been active for at least 1 Myr and are featured by only several datable events, representing co-seismic motions on the faults.

5 Discussion

Onset of extensional tectonics in the Alps has remained a topic of debate for the last 20 years. A Miocene age has been proposed for the onset of the extensional activation of the PFT based on AFT dating on both sides of this major fault, i.e. in the Pelvoux external crystalline massif and in the Champsaur sandstones to the west and in the Briançonnais zone to the east (Tricart et al., 2001, 2007; Beucher et al., 2012). The Briançonnais zone corresponds to the east hang-

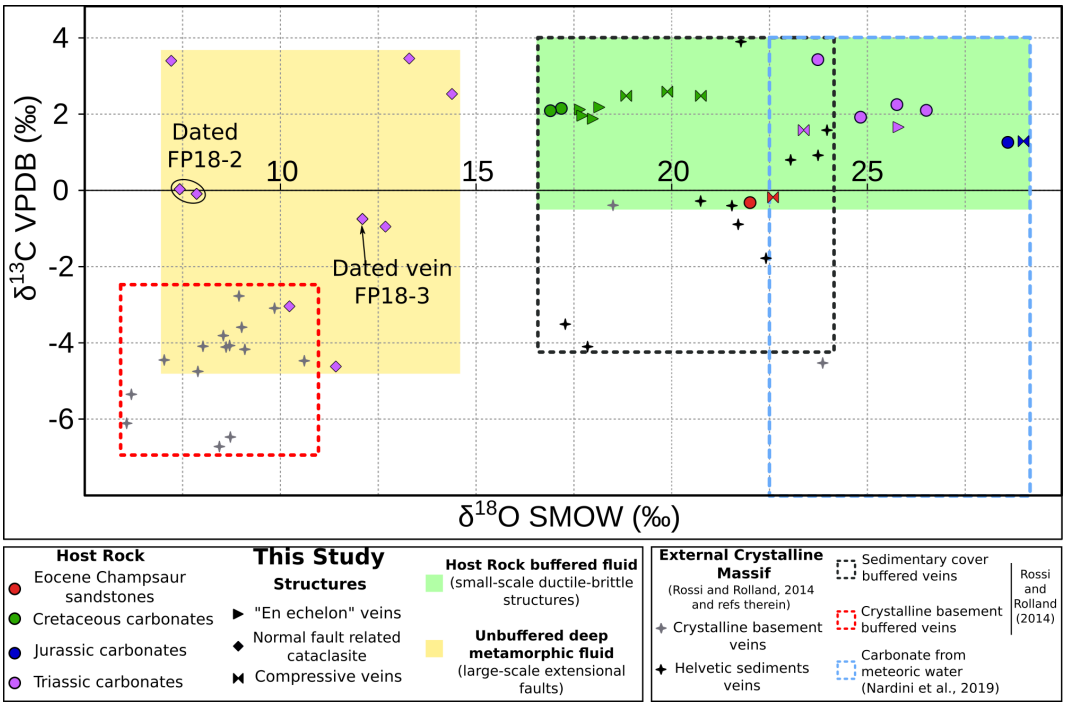

Figure 6. Stable isotopic data from samples indicated in Fig. 2. Domains represented by dashed red, black and blue lines are from the literature (Nardini et al., 2019; Rossi and Rolland, 2014, and references therein). The green domain corresponds to veins associated with brittle–ductile structures. These veins show similar isotopic compositions to their host rocks. The orange domain features the signature of cataclased normal fault samples, which show a different isotopic composition as compared to their host rock and are similar to deep metamorphic fluids (e.g. Crespo-Blanc et al., 1995; Rossi and Rolland, 2014; Rolland and Rossi, 2016).

ing wall compartment of the PFT. In this compartment, AFT ages ranging from 30 to 20 Ma are interpreted as the exhumation age of this area related to the compressional activity of the PFT during the Alpine collision, the motion of which is constrained by direct $^{40}Ar/^{39}Ar$ dating on phengite at 35–25 Ma (Simon-Labric et al., 2009; Bellanger et al., 2015). To the west (footwall of the PFT), the AFT ages range from 13 to 4 Ma in the Pelvoux external crystalline massif (Beucher et al., 2012) and from 9 to 4 Ma in the Champsaur sandstones (Tricart et al., 2007), and are interpreted as the extensional reactivation of the PFT by the latter authors. As the AFT dates record an exhumation age associated with cooling below $\sim 100\,°C$ (Ault et al., 2019), they may not correspond to an age of PFT activity but rather record an erosion process that is related to both climatic and tectonic processes (e.g. Champagnac et al., 2007). Sternai et al. (2019) suggest that vertical movement in the Western Alps may be mainly ascribed to erosion and deglaciation (Nocquet et al., 2016) and may also include a significant mantle convection component (Salimbeni et al., 2018). However, the external crystalline massifs exhumation was also driven by frontal thrusting activated during the middle Miocene at the western front of these massifs (Boutoux et al., 2016) and by strong erosional processes that enhanced exhumation beginning in the late Miocene (Cederbom et al., 2004). Along the PFT, younger AFT and phengite $^{40}Ar/^{39}Ar$ ages of ~ 10 Ma were obtained on the Plan de Phasy (Guillestre) metagranite mylonites (Tricart et al., 2007; Lanari et al., 2014). These ages have been interpreted as the result of hydrothermal fluid circulation, which may be linked to tectonic activity of the High Durance fault system. However these fluid circulations may be passive through the PFT network and may not correspond to extension onset. Therefore, the age of PFT activity remains unconstrained and requires some direct dating. In the following discussion, we show how absolute U–Pb dating of fracture infill calcite brings quantitative time constraints on PFT fault movement.

5.1 Deformation and scale of fluid flow in the brittle–ductile structures

The measured $\delta^{18}O$ and $\delta^{13}C$ isotope ratios of veins from brittle–ductile structures are close or similar to their host rocks and remain close to the field of carbonates precipitated from meteoric water (Sect. 4.2). Based on several studies in the frontal parts of Alpine orogens (Smeraglia et al., 2020; Nardini et al., 2019), these isotope signatures are thought to be representative of meteoric water inflow from the most superficial domains. Three important parameters are involved to control this surface-derived fluid regime: (i) lack of large-scale structures, (ii) pressure-solution microstructures (evi-

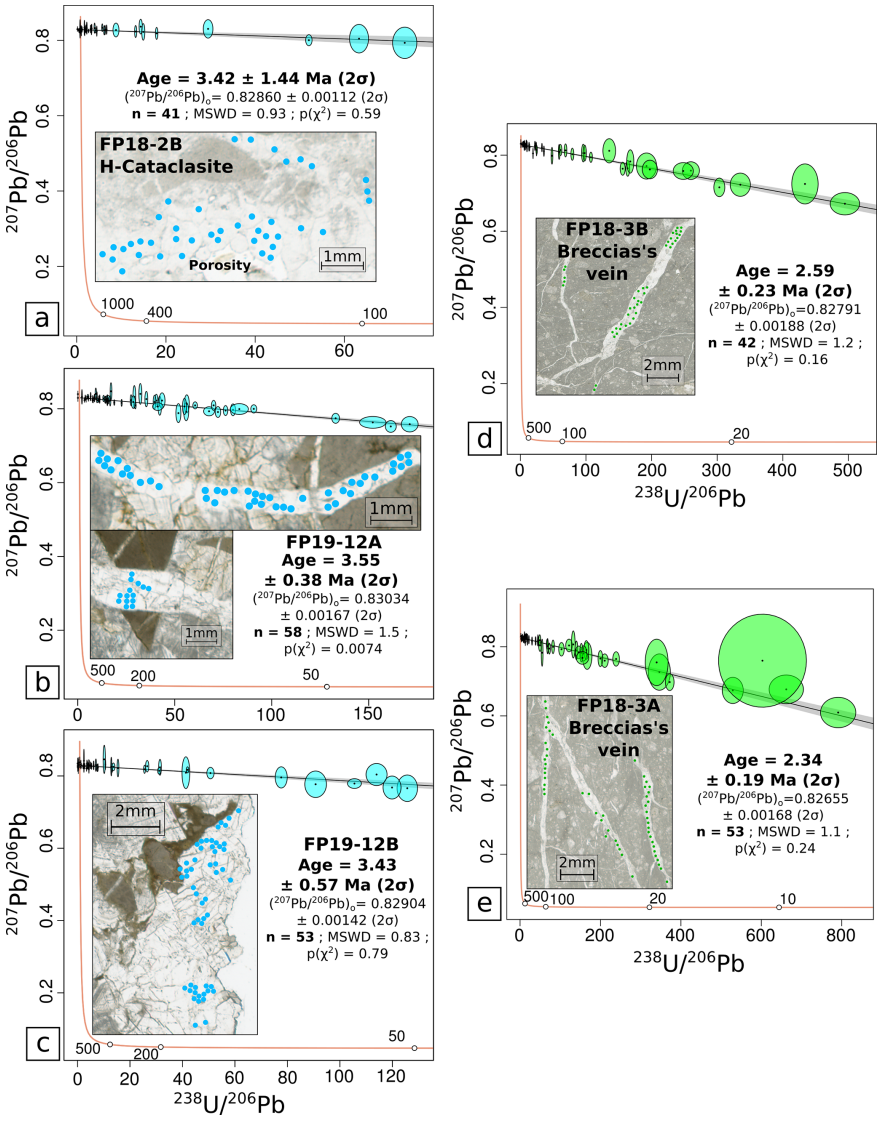

Figure 7. Tera-Wasserburg concordia plot of **(a)** highly cataclased sample FP18-2 calcite filling, **(b, c)** sample FP19-12A veins and FP19-12A "clean calcite" filling, and **(d, e)** sample FP18-3 veins and corresponding maps of sampled spots (150 µm). MSWD: mean square weighted deviation. An additional error propagation tied to WC-1 standard uncertainty is taken into account.

dence of local fluid) and (iii) presence of shallow impermeable clay-rich layers which isolate upper crust from more deeply rooted systems (Sect. 4.1. and Fig. 3). Rossi and Rolland (2014) report similar stable isotope signatures in the Mont Blanc external crystalline massif sedimentary cover (Helvetic schists). There, the vein calcites bear similar stable isotope values to the host Helvetic schists, which is in agreement with the fluids having equilibrated with their host rocks in a closed system with low fluid / rock ratios (Rolland and Rossi, 2016). In our study, observations of veins show that they were closely related to schistosity acting as a stylolithic dissolution surface (Sect. 4.1). This observation is consistent with local fluid interactions and equilibrium with the host rock, resulting from a pressure–dissolution–recrystallization transfer mode (e.g. Passchier and Throw, 2005). Based on this, we suggest that the external fluid signature was buffered by the host rock signature. These fluid compositions show that en-echelon veins are linked to an early deformation, where the porosity was still not connected by the fault network (Fig. 3). In such a system, the veins kept the host rock signature, and no crustal-scale fluid flow circulation is evidenced.

5.2 Scale of fluid flow in the brittle extensional structures

Major (> metre-scale width) faults are related to shallower or higher stress contexts (e.g. Passchier and Throw, 2005).

The isotopic composition of calcite that crystallized in these brittle extensional faults is significantly different from their host rock (Sect. 4.2; Fig. 6). Indeed, calcites related to these major faults have a 10 ‰ lower $\delta^{18}O$ than their host rock and a $\delta^{13}C$ ranging between −5 and 4 ‰ PDB (while the $\delta^{13}C$ ratio of Triassic host rock is 2 ‰). This signature is similar to that of exogenous metamorphic fluid origin (Crespo-Blanc et al., 1995; Rossi and Rolland, 2014). The observed CL pattern of calcites also argues for variations in the fluid composition, between the different veins and progressively within a given vein. Similar signatures are recorded in the Mont Blanc external crystalline massif shear zones and veins in a similar structural context (Rossi et al., 2014). There, a similar spread of $\delta^{13}C$–$\delta^{18}O$ values is observed in the marginal part of the crystalline basement, at the contact with the Helvetic schists. This spread is interpreted as a mixing between fluids flowing down through the sedimentary cover and fluids flowing upwards originating from shear zones in the Mont Blanc massif (Rolland and Rossi, 2016). The chemical signature of calcite veins in the Massif Central shear zones is correlated to a Mg–K-rich metasomatism, both arguing for CO_2-bearing fluids representative of a deep source, which is rooted in the mantle via vertical shear zones (Rossi et al., 2005). This deeply rooted fluid cell is also suggested by fluids significantly hotter (150–250 °C) than their host rock at ca. 10 Ma along vertical faults in the Belledonne massif, which are in continuity with the central Mont Blanc massif shear zones (Janots et al., 2019). Indeed, deep metamorphic fluid circulation is in good agreement with a crustal-scale fluid pathway which is activated during the extensional motion of the PFT, connected to the Rhône–Simplon right-lateral fault (Bergemann et al., 2019, 2020). This crustal-scale network suggests that extensional faults connected to the PFT in depth when it was reactivated as a detachment. Deep connection with the PFT crustal-scale structure (e.g. Sue et al., 2003) would allow fluid circulation from the interface of European slab with the deep subduction and collisional metamorphosed prism. In our study, the isotopic dataset shows a significant difference between the deep fluid signature recorded by the Mont Blanc veins (Rossi and Rolland, 2014; Rolland and Rossi, 2016) and the compositions of the veins related to brittle–ductile structures (Fig. 6). This variability suggests a mixing process between the local fluids trapped in the early extensional features (closed system) and these exogenous fluids from a deep crustal origin.

5.3 Timing of PFT extensional inversion

All ages obtained from the investigated Tournoux normal fault scarps give direct time constraints on the final stages of extensional slip and are interpreted as a minimum age for the extensional reactivation of the PFT. The oldest event is the formation of the highly deformed cataclasite calcite filling and veins ∼ 3.5 Ma (3.4 ± 1.5, 3.6 ± 0.4 and 3.4 ± 0.6 Ma). This calcitic cementation occurred directly after the main cataclastic deformation event and before the late cross-cutting veins. Latter cross-cutting veins gave the same ∼ 2.5 Ma age, with two within-error dates of 2.6 ± 0.3 and 2.3 ± 0.3 Ma. The ∼ 3.5 and ∼ 2.5 Ma ages do not represent the same slip event on the fault. It is noteworthy that all these ages are calculated assuming secular equilibrium in the U-series decay chain. As fluids are generally characterized by an excess in ^{234}U with respect to ^{238}U, resulting in an excess of radiogenic ^{206}Pb, the calculated ages should be considered as maximum ages (see for example Walker et al., 2006). The magnitude of the offset ages due to initial $^{234}U/^{238}U$ disequilibrium can be significant, and the true age could be younger by several hundreds of thousands of years. In the present case, it was not possible to carry out classical isotopic analyses of uranium by isotopic dilution to measure any detectable residual $^{234}U/^{238}U$ disequilibrium because of the size of the carbonate phases. It could be hazardous to speculate on the initial $^{234}U/^{238}U$ disequilibria of the fluids, but the quite high uranium concentrations (up to the ppm level) observed in analysed minerals of samples FP18-2 and FP18-3 (Fig. 7) are likely indicative of an oxidizing environment and thus of a moderate initial ^{234}U excess (Walker et al., 2006). To assess the impact of this excess on the final age, we have tested various initial $^{234}U/^{238}U$ activity ratios ranging between 1 and 2 as illustrated in Fig. 8. For an initial ($^{234}U/^{238}U$) activity ratio of 2, the true age is lower by about ∼ 370 kyr. The obtained ages assuming an initial ($^{234}U/^{238}U$) ratio of 1 are thus regarded as maximum ages.

As they remain undeformed, the latter veins are considered as the youngest tectonic slip along the fault. Furthermore, the geometry of the Tournoux normal fault regarding the PFT position indicates that this normal fault was connected to the PFT, which acted as a detachment zone (Fig. 9). Thus, it may represent the palaeo-HDFS seismogenic zone, which was later exhumed in the footwall part of the active extensional fault. The main activity of this palaeo-fault can be bracketed between 3.4 and 2.2 Ma based on the above results.

5.4 Evolution of PFT through time

The structural and dating results presented in this paper, combined with the literature on PFT footwall and hanging wall exhumation, lead to the following reconstitution of its evolution (Fig. 9).

The investigated PFT palaeoseismic zone is located 3 to 10 km west of the active HDFS seismogenic zone. At present day, the extensional deformation is mainly localized on one active fault and mostly occurs between 3 and 8 km depth (Sue et al., 2007; Mathey et al., 2020). This study gives insights into the uplift rate and lateral displacement of the High Durance fault system footwall and hanging wall since the passage of the investigated palaeo-PFT through the upper boundary of the seismogenic crust some 2–3.5 Myr ago. Since then, the PFT hanging wall, represented by the active

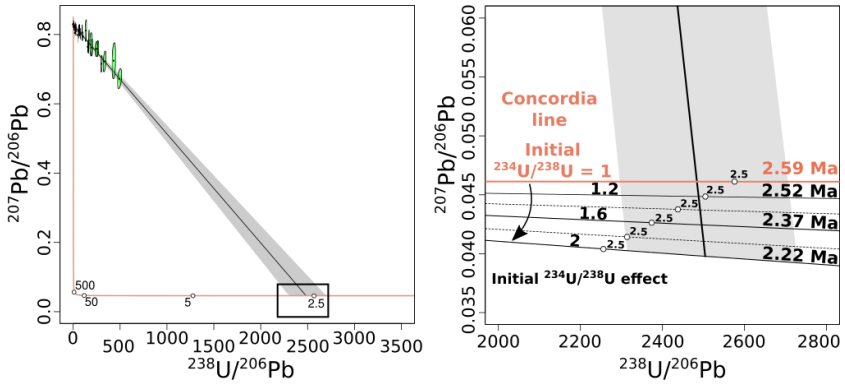

Figure 8. Impact of the initial ^{234}U excess on the final age estimation. Several initial $^{234}U/^{238}U$ activity ratios have been tested ranging between 1 and 2. This spread in initial $^{234}U/^{238}U$ leads to an age difference of 0.37 Ma. The obtained U / P age of 2.59 Ma, assuming equality of ^{234}U and ^{238}U contents, is thus a maximum age.

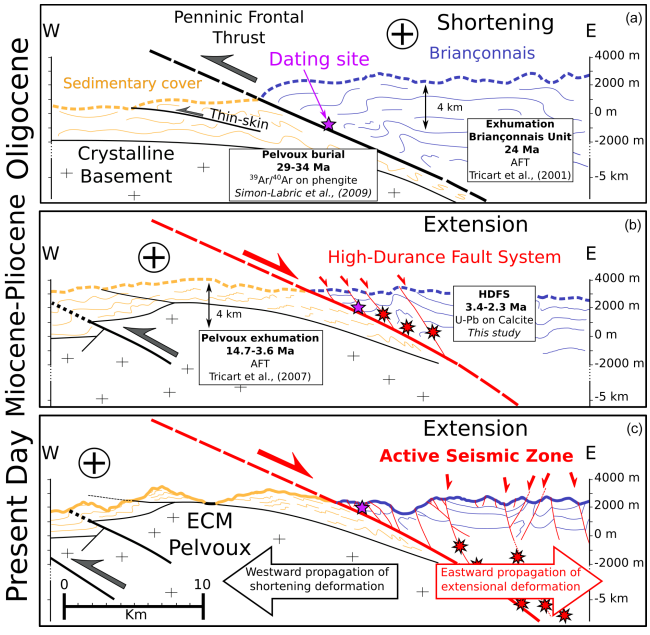

Figure 9. Evolutionary geological cross-section sketch of PFT; position and geometry of main faults from Tricart et al. (2006). **(a)** Compressional activation of the PFT resulting in joint external crystalline massif burial and Briançonnais exhumation during the Oligocene. **(b)** Extensional reactivation of the PFT and setting up of the High Durance fault system during the Pliocene as evidenced in this study. At this point the dated extensional fault passes through the upper boundary of the seismic zone at ca. 2–3 Ma. **(c)** At present day, compressional deformation has migrated westward (frontal part of external crystalline massifs, since ca. 15 Ma), and extensional seismic activity of the High Durance fault system is recorded at shallow depth 3–10 km east of the studied palaeoseismic zone.

extensional deformation front of the HDFS, was significantly shifted eastward, while its footwall was uplifted up to 3 km (Fig. 9). This leads to a mean vertical tectonic motion of the order of $> 1\,\mathrm{mm\,yr^{-1}}$ for the footwall compartment of PFT in this period of time. This rate is consistent with the vertical GPS rates measured for the Pelvoux external crystalline massif (Nocquet et al., 2016; Sternai et al., 2019).

Our data support the hypothesis that the present HDFS is the result of eastward shifting of extensional deformation, accommodated by successive jumps on several faults. Faults were likely active on a scale of ≥ 1 Myr before becoming inactive. Calcite U–Pb ages obtained on the Tournoux scarp constrain co-seismic motion on two conjugate faults. The two age groups obtained on these extensional faults connected to the PFT highlight at least two phases of deformation, at 3.5 ± 0.4 Ma and one or two discrete brittle events at, or within, 2.6 ± 0.2 and 2.3 ± 0.2 Ma, which gives insights into the long-term activity of at least 1 Myr, but with only several datable events, which argues for an apparent contradiction. Indeed, co-seismic displacement on the fault suggests a significant magnitude for the related earthquake (Wells and Coppersmith, 1994), which is apparently incompatible with the very few datable motions. This gives some weight to a deformation regime which may alternate long phases of creeping on the fault plane, without any brittle deformation, with very rare phases of brittle deformation.

The vertical uplift and exhumation of the Pelvoux external massif since 3.5 Ma may thus mainly result from the cumulated fault motion on these several fault segments. These data are thus in agreement with a significant tectonic component in the measured uplift signal of external crystalline massifs, which is in agreement with a clear difference in uplift rates measured between ECMs and the internal Alps (Nocquet et al., 2016; Sternai et al., 2019).

We support the hypothesis that the HDFS is the result of the eastward extensional deformation shift and the successive activation of faults, which incrementally participated in the exhumation of the western (Pelvoux) footwall side of the fault system.

6 Conclusion

Significant constraints on the evolution of fault systems can be acquired by coupling stable isotopic analysis and U–Pb dating on calcite. These methods have been successfully applied to unravel the tectonic reactivation of the PFT for the first time. Five U–Pb ages of calcite have been obtained in extensional fault structures connected to the PFT, giving two distinct groups of ages of 3.5 ± 0.5 Ma for the main deformation phase represented by the cataclasite calcite cement, cross-cut by later discrete phases represented by millimetre-large veins dated from 2.6 ± 0.3 to 2.3 ± 0.3 Ma. The 3.5 Ma age represents a minimum age for the onset of extensional brittle reactivation of the PFT. Earliest extensional ductile–brittle structures cannot be dated due to low uranium contents and low U / Pb ratios. Associated with those two (ductile and brittle) deformation stages, stable isotopic ratios of carbon (δ^{13}C) and oxygen (δ^{18}O) of calcite samples collected within the kilometre-scale extensional faults show an evolution from a closed to an open fluid system. The isotopic signature of fluids related to the brittle deformation stage corresponds an open system due to the activation of a crustal-scale fluid circulation cell when the HDFS developed in connection with the deeper PFT deeper structure. The fluids associated with this open system show a deep crustal and/or mantle signature similar to that measured along the PFT across the Alpine arc. This deeply rooted upward fluid circulation occurred when extensional fault activity was connected to the PFT reactivated as a detachment, which suggests a crustal-scale extensional reactivation at this stage. These constraints on the PFT fluid regime are the first direct evidence for a transition towards a crustal-scale fluid regime at the onset of brittle extensional reactivation in the Alps. The direct ages of PFT motion give insights into the long-term incremental displacement of the HDFS footwall and Pelvoux massif exhumation, which corresponds to its passage through the upper part of the seismogenic zone, at a mean rate of $> 1\,\mathrm{mm\,yr^{-1}}$ in the last 3 Myr.

Data availability. All the data are available in the Supplement.

Supplement. The supplement related to this article is available online at: https://doi.org/10.5194/se-12-237-2021-supplement.

Author contributions. AB, YR and SS wrote the manuscript, and all authors discussed the results and contributed to the final article. TD supported AB for map creation and cross sections. YR, SS, TD, CG and AB participated in field trip sampling. AB did the sample petrographic characterization with optical microscope and cathodoluminescence. NG, AG and PD led U–Pb dating with AB. BB and AN supervised AB in stable isotope analysis, for result interpretation and protocol application, respectively.

Competing interests. The authors declare that they have no conflict of interest.

Special issue statement. This article is part of the special issue "New insights on the tectonic evolution of the Alps and the adjacent orogens". It is not associated with a conference.

Acknowledgements. This work forms part of first author's PhD, funded by the Bureau de Recherches Géologiques et Minières (BRGM) in the frame of the RGF-ALPES-BRGM-2019 project. The CEREGE group is supported by two French "Investissements d'Avenir" funding associations: the EQUIPEX-ASTER-CEREGE and the Initiative d'Excellence of Aix-Marseille University – A*Midex, through the DatCarb project. We wish to thank Fayçal Soufi for his help in sample preparation.

Many thanks are due to Alfons Berger, one anonymous reviewer and Giancarlo Molli for their constructive comments, which improved the manuscript.

Financial support. This research has been supported by the Bureau de Recherches Géologiques et Minières (grant no. RGF-ALPES-BRGM-2019), the EQUIPEX-ASTER-CEREGE and the Initiative d'Excellence of Aix-Marseille University – A*Midex, through the DatCarb project.

Review statement. This paper was edited by Giancarlo Molli and reviewed by Alfons Berger and one anonymous referee.

References

Agard, P., Monie, P., Jolivet, L., and Goffé, B.: Exhumation of the Schistes Lustre´s complex: in situ laser probe 40Ar/39Ar constraints and implications for the Western Alps, J. Metamorphic Geol., 20, 599–618, https://doi.org/10.1046/j.1525-1314.2002.00391.x, 2002.

Andrieu, S., Brigaud, B., Rabourg, T., and Noret, A.: The Mid-Cenomanian Event in shallow marine environments: Influence on carbonate producers and depositional sequences (northern Aquitaine Basin, France), Cretaceous Res., 56, 587–607, https://doi.org/10.1016/j.cretres.2015.06.018, 2015.

Ault, A. K., Gautheron, C., and King, G. E.: Innovations in (U–Th)/He, fission track, and trapped charge thermochronometry with applications to earthquakes, weathering, surface-mantle connections, and the growth and decay of mountains, Tectonics, 38, 3705–3739, https://doi.org/10.1029/2018TC005312, 2019.

Barnaby, R. J. and Rimstidt, J. D.: Redox conditions of calcite cementation interpreted from Mn and Fe contents of authigenic calcites, Geol. Soc. Am. Bull., 101, 795–804, https://doi.org/10.1130/0016-7606(1989)101<0795:RCOCCI>2.3.CO;2, 1989.

Beaudoin, N., Huyghe, D., Bellahsen, N., Lacombe, O., Emmanuel, L., Mouthereau, F., and Ouanhnon, L.: Fluid systems and fracture development during syn-depositional fold growth:

An example from the Pico del Aguila anticline, Sierras Exteriores, southern Pyrenees, Spain, J. Struct. Geol., 70, 23–38, https://doi.org/10.1016/j.jsg.2014.11.003, 2015.

Beaudoin, N., Lacombe, O., Roberts, N. M. W., and Koehn, D.: U-Pb dating of calcite veins reveals complex stress evolution and thrust sequence in the Bighorn Basin, Wyoming, USA, Geology, 46, 1015–1018, https://doi.org/10.1130/G45379.1, 2018.

Bellahsen, N., Mouthereau, F., Boutoux, A., Bellanger, M., Lacombe, O., Jolivet, L., and Rolland, Y.: Collision kinematics in the western external Alps, Tectonics, 33, 1055–1088, https://doi.org/10.1002/2013TC003453, 2014.

Bellanger, M., Augier, R., Bellahsen, N., Jolivet, L., Monié, P., Baudin, T., and Beyssac, O.: Shortening of the European Dauphinois margin (Oisans Massif, Western Alps): New insights from RSCM maximum temperature estimates and $^{40}Ar/^{39}Ar$ in situ dating, J. Geodyn., 83, 37–64, https://doi.org/10.1016/j.jog.2014.09.004, 2015.

Beltrando, M., Lister, G. S., Forster, M., Dunlap, W. J., Fraser, G., and Hermann, J.: Dating microstructures by the $^{40}Ar/^{39}Ar$ step-heating technique: Deformation–pressure–temperature–time history of the Penninic Units of the Western Alps, Lithos, 113, 801–819, https://doi.org/10.1016/j.lithos.2009.07.006, 2009.

Bergemann, C. A., Gnos, E., and Whitehouse, M. J.: Insights into the tectonic history of the Western Alps through dating of fissure monazite in the Mont Blanc and Aiguilles Rouges Massifs, Tectonophysics, 750, 203–212, https://doi.org/10.1016/j.tecto.2018.11.013, 2019.

Bergemann, C. A., Gnos, E., Berger, A., Janots, E., and Whitehouse, M. J.: Dating tectonic activity in the Lepontine Dome and Rhone-Simplon Fault regions through hydrothermal monazite-(Ce), Solid Earth, 11, 199–222, https://doi.org/10.5194/se-11-199-2020, 2020.

Bertrand, A. and Sue, C.: Reconciling late faulting over the whole Alpine belt: from structural analysis to geochronological constrains, Swiss J. Geosci., 110, 565–580, https://doi.org/10.1007/s00015-017-0265-4, 2017.

Beucher, R., van der Beek, P., Braun, J., and Batt, G. E.: Exhumation and relief development in the Pelvoux and Dora-Maira analysis and inversion of thermochronological age transects, J. Geophys. Res., 117, F03030, https://doi.org/10.1029/2011JF002240, 2012.

Bons, P. D., Elburg, M. A., and Gomez-Rivas, E.: A review of the formation of tectonic veins and their microstructures, J. Struct. Geol., 43, 33–62, https://doi.org/10.1016/j.jsg.2012.07.005, 2012.

Boutoux, A., Bellahsen, N., Nanni, U., Pik, R., Verlaguet, A., Rolland, Y., and Lacombe, O.: Thermal and structural evolution of the external Western Alps: Insights from (U–Th–Sm)/He thermochronology and RSCM thermometry in the Aiguilles Rouges/Mont Blanc massifs, Tectonophysics, 683, 109–123, https://doi.org/10.1016/j.tecto.2016.06.010, 2016.

Cederbom, C. E., Sinclair, H. D., Schlunegger, F., and Rahn, M. K.: Climate induced rebound and exhumation of European Alps, Geology, 32, 709–712, https://doi.org/10.1130/G20491.1, 2004.

Cenki-Tok, B., Darling, J. R., Rolland, Y., Dhuime, B., and Storey, C. D.: Direct dating of mid-crustal shear zones with synkinematic allanite: new in situ U-Th-Pb geochronological approaches applied to the Mont Blanc massif, Terra Nova, 26, 29–37, https://doi.org/10.1111/ter.12066, 2014.

Ceriani, S. and Schmid, S. M.: From N-S collision to WNW-directed post-collisional thrusting and folding: Structural study of the Frontal Penninic Units in Savoie (Western Alps, France), Eclogae Geol. Helv., 97, 347–369, https://doi.org/10.1007/s00015-004-1129-2, 2004.

Ceriani, S., Fügenschuh, B., and Schmid, S. M.: Multi-stage thrusting at the "Penninic Front" in the Western Alps between Mont Blanc and Pelvoux massifs, Int. J. Earth Sci., 90, 685–702, https://doi.org/10.1007/s005310000188, 2001.

Champagnac, J. D., Molnar, P., Anderson, R. S., Sue, C., and Delacou, B.: Quaternary erosion-induced isostatic rebound in the western Alps, Geology, 35, 195–198, https://doi.org/10.1130/G23053A.1, 2007.

Crespo-Blanc, A., Masson, H., Sharp, Z., and Cosca, M.: A stable and $^{40}Ar/^{39}Ar$ isotope study of a major thrust in the Helvetic nappes (Swiss Alps): Evidence for fluid flow and constraints on nappe kinematics, Geol. Soc. Am. Bull., 107, 1129–1144, https://doi.org/10.1130/0016-7606(1995)107<1129:ASAAAI>2.3.CO;2, 1995.

Duchêne, S., Blichert-Toft, J., Luais, B., Télouk, P., Lardeaux, J.-M., and Albarède, F.: The Lu–Hf dating of garnets and the ages of the Alpine high-pressure metamorphism, Nature, 387, 586–589, https://doi.org/10.1038/42446, 1997.

Dumont, T., Schwartz, S., Guillot, S., Simon-Labric, T., Tricart, P., and Jourdan, S.: Structural and sedimentary records of the Oligocene revolution in the Western Alpine arc, J. Geodyn., 56–57, 18–38, https://doi.org/10.1016/j.jog.2011.11.006, 2012.

Goodfellow, B. W., Viola, G., Bingen, B., Nuriel, P., and Kylander-Clark, A. R. C.: Palaeocene faulting in SE Sweden from U-Pb dating of slickenfibre calcite, Terra Nova, 29, 321–328, https://doi.org/10.1111/ter.12280, 2017.

Janots, E., Grand'Homme, A., Bernet, M., Guillaume, D., Gnos, E., Boiron, M.-C., Rossi, M., Seydoux-Guillaume, A.-M., and De Ascenção Guedes, R.: Geochronological and thermometric evidence of unusually hot fluids in an Alpine fissure of Lauzière granite (Belledonne, Western Alps), Solid Earth, 10, 211–223, https://doi.org/10.5194/se-10-211-2019, 2019.

Jochum, K. P., Weis, U., Stoll, B., Kuzmin, D., Yang, Q., Raczek, I., Jacob, D. E., Stracke, A., Birbaum, K., Frick, D. A., Günther, D., and Enzweiler, J.: Determination of reference values for NIST SRM 610–617 glasses following ISO guidelines, Geostand. Geoanal. Res., 35, 397–429, https://doi.org/10.1111/j.1751-908X.2011.00120.x, 2011.

Kim, S.-T., Coplen, T. B., and Horita, J.: Normalization of stable isotope data for carbonate minerals: Implementation of IUPAC guidelines, Geochim. Cosmochim. Ac., 158, 276–289, https://doi.org/10.1016/j.gca.2015.02.011, 2015.

Lanari, P., Guillot, S., Schwartz, S., Vidal, O., Tricart, P., Riel, N., and Beyssac, O.: Diachronous evolution of the alpine continental wedge: evidences from P-T estimates in the Briançonnais Zone houillère (France-Western Alps), J. Geodyn., 56-57, 39–54, https://doi.org/10.1016/j.jog.2011.09.006, 2012.

Lanari, P., Rolland, Y., Schwartz, S., Vidal, O., Guillot, S., Tricart, P., and Dumont, T.: P-T-t estimation of syn-kinematic strain in low-grade rocks ($< 300\,^{\circ}C$) using thermodynamic modelling and $^{40}Ar/^{39}Ar$ dating techniques: example of the Plan-de-Phasy shear zone (Briançonnais Zone, Western Alps), Terra Nova, 26, 130–138, https://doi.org/10.1111/ter.12079, 2014.

Lardeaux, J. M., Schwartz, S., Tricart, P., Paul, A., Guillot, S., Béthoux, N., and Masson, F.: A crustal-scale cross-section of the southwestern Alps combining geophysical and geological imagery, Terra Nova, 18, 412–422, https://doi.org/10.1111/j.1365-3121.2006.00706.x, 2006.

Larroque, C., Delouis, B., Godel, B., and Nocquet, J.-M.: Active deformation at the southwestern Alps–Ligurian basin junction (France–Italy boundary): Evidence for recent change from compression to extension in the Argentera massif, Tectonophysics, 467, 22–34, https://doi.org/10.1016/j.tecto.2008.12.013, 2009.

Malusà, M., Zhao, L., Eva, E., Solarino, S., Paul, A., Guillot, S., Schwartz, S., Dumont, T., Aubert, C., Salimbeni, S., Pondrelli, S., Wang, Q., and Zhu, R.: Earthquakes in the western alpine mantle wedge, Gondwana Res., 44, 89–95, https://doi.org/10.1016/j.gr.2016.11.012, 2017.

Mathey, M., Walpersdorf, A., Sue, C., Baize, S., and Deprez, A.: Seismogenic potential of the High Durance Fault constrained by 20 yr of GNSS measurements in the Western European Alps, Geophy. J. Int., 222, 2136–2146, https://doi.org/10.1093/gji/ggaa292, 2020.

Mugnier, J. L., Loubat, H., and Cannic, S.: Correlation of seismic images and geology at the boundary between internal and external domains of the Western Alps, Bull. Soc. Géol. Fr., 164, 697–708, 1993.

Nardini, N., Muñoz-López, D., Cruset, D., Cantarero, I., Martín-Martín, J., Benedicto, A., Gomez-Rivas, E., John, C., and Travé, A.: From Early Contraction to Post-Folding Fluid Evolution in the Frontal Part of the Bóixols Thrust Sheet (Southern Pyrenees) as Revealed by the Texture and Geochemistry of Calcite Cements, Minerals, 9, 117–146, https://doi.org/10.3390/min9020117, 2019.

Nocquet, J. M., Sue, C., Walpersdorf, A., Tran, T., Lenôtre, N., Vernant, P., Cushing, M., Jouanne, F., Masson, F., Baize, S., Chéry, J., and Van der Beek, P. A.: Present-day uplift of the western Alps, Sci. Rep., 6, 1–6, https://doi.org/10.1038/srep28404, 2016.

Passchier, C. W. and Trouw, R. A. J.: Microtectonics, 2nd rev. edn., Springer, Berlin, Germany, New York, USA, 2005.

Paton, C., Hellstrom, J., Paul, B., Woodhead, J., and Hergt, J.: Iolite: Freeware for the visualisation and processing of mass spectrometric data, J. Anal. Atom. Spectrom., 26, 2508–2518, https://doi.org/10.1039/c1ja10172b, 2011.

Ring, U. and Gerdes, A.: Kinematics of the Alpenrhein-Bodensee graben system in the Central Alps: Oligocene/Miocene transtension due to formation of the Western Alps arc, Tectonics, 35, 1367–1391, https://doi.org/10.1002/2015TC004085, 2016.

Roberts, N. M. W., Rasbury, E. T., Parrish, R. R., Smith, C. J., Horstwood, M. S. A., and Condon, D. J.: A calcite reference material for LA-ICP-MS U-Pb geochronology: Calcite RM for LA-ICP-MS U-Pb dating, Geochem. Geophy. Geosy., 18, 2807–2814, https://doi.org/10.1002/2016GC006784, 2017.

Roberts, N. M. W., Drost, K., Horstwood, M. S. A., Condon, D. J., Chew, D., Drake, H., Milodowski, A. E., McLean, N. M., Smye, A. J., Walker, R. J., Haslam, R., Hodson, K., Imber, J., Beaudoin, N., and Lee, J. K.: Laser ablation inductively coupled plasma mass spectrometry (LA-ICP-MS) U–Pb carbonate geochronology: strategies, progress, and limitations, Geochronology, 2, 33–61, https://doi.org/10.5194/gchron-2-33-2020, 2020.

Rolland, Y. and Rossi, M.: Two-stage fluid flow and element transfers in shear zones during collision burial-exhumation cycle: Insights from the Mont Blanc Crystalline Massif (Western Alps), J. Geodyn., 101, 88–108, https://doi.org/10.1016/j.jog.2016.03.016, 2016.

Rolland, Y., Rossi, M., Cox, S. F., Corsini, M., Mancktelow, N., Pennacchioni, G., Fronari, M., and Boullier, A. M.: $^{40}Ar/^{39}Ar$ dating of synkinematic white mica: insights from fluid-rock reaction in low-grade shear zones (Mont Blanc Massif) and constraints on timing of deformation in the NW external Alps, Geol. Soc. Lond., Special Publications, 299, 293–315, https://doi.org/10.1144/SP299.18, 2008.

Rossi, M. and Rolland, Y.: Stable isotope and Ar/Ar evidence of prolonged multiscale fluid flow during exhumation of orogenic crust: Example from the Mont Blanc and Aar Massifs (NW Alps): Multi-scale fluid flow in the Alps, Tectonics, 33, 1681–1709, https://doi.org/10.1002/2013TC003438, 2014.

Rossi, M., Rolland, Y., Vidal, O., and Cox, S. F.: Geochemical variations and element transfer during shear-zone development and related episyenites at middle crust depths: insights from the Mont Blanc granite (French-Italian Alps), Geol. Soc. Lond., Special Publications, 245, 373–396, https://doi.org/10.1144/GSL.SP.2005.245.01.18, 2005.

Rothé, E.: La seismicité des Alpes occidentales, B. Soc. Géol. Fr., 5, 295–320, 1942.

Rubatto, D. and Hermann, J.: Zircon formation during fluid circulation in eclogites (Monviso, Western Alps): implications for Zr and Hf budget in subduction zones, Geochim. Cosmochim. Ac., 67, 2173–2187, https://doi.org/10.1016/S0016-7037(02)01321-2, 2003.

Salimbeni, S., Zhao, L., Malusà, M., Guillot, S., Pondrelli, S., Margheriti, L., Paul, A., Solarino, S., Aubert, C., Dumont, T., Schwartz, S., Wang, Q., Xu, X., Zheng, T., and Zhu, R.: Fossil and active mantle flows in the western Alpine region unravelled by seismic anisotropy analysis and high-resolution P wave tomography, Tectonophysics, 731–732, 35–47, https://doi.org/10.1016/j.tecto.2018.03.002, 2018.

Sanchez, G., Rolland, Y., Schneider, J., Corsini, M., Oliot, E., Goncalves, P., Verati, C., Lardeaux, J.-M., and Marquer, D.: Dating low-temperature deformation by $^{40}Ar/^{39}Ar$ on white mica, insights from the Argentera-Mercantour Massif (SW Alps), Lithos, 125, 521–536, https://doi.org/10.1016/j.lithos.2011.03.009, 2011.

Schmid, S. M. and Kissling, E.: The arc of the western Alps in the light of geophysical data on deep crustal structure, Tectonics, 19, 62–85, https://doi.org/10.1029/1999TC900057, 2000.

Schwartz, S., Lardeaux, J. M., Tricart, P., Guillot, S., and Labrin, E.: Diachronous exhumation of HP-LT metamorphic rocks from south-western Alps: evidence from fission-track analysis, Terra Nova, 19, 133–140, https://doi.org/10.1111/j.1365-3121.2006.00728.x, 2007.

Schwartz, S., Gautheron, C., Audin, L., Dumont, T., Nomade, J., Barbarand, J., Pinna-Jamme, R., and van der Beek, P.: Foreland exhumation controlled by crustal thickening in the Western Alps, Geology, 45, 139–142, https://doi.org/10.1130/G38561.1, 2017.

Seward, D. and Mancktelow, N. S.: Neogene kinematics of the central and western Alps: Evidence from fission-track dating, Geology, 22, 803–806, https://doi.org/10.1130/0091-7613(1994)022<0803:NKOTCA>2.3.CO;2, 1994.

Simon-Labric, T., Rolland, Y., Dumont, T., Heymes, T., Authemayou, C., Corsini, M., and Fornari, M.: $^{40}Ar/^{39}Ar$ dat-

ing of Penninic Front tectonic displacement (W Alps) during the Lower Oligocene (31–34 Ma), Terra Nova, 21, 127–136, https://doi.org/10.1111/j.1365-3121.2009.00865.x, 2009.

Smeraglia, L., Fabbri, O., Choulet, F., Buatier, M., Boulvais, P., Bernasconi, S. M., and Castorina, F.: Syntectonic fluid flow and deformation mechanisms within the frontal thrust of a foreland fold-and-thrust belt: Example from the Internal Jura, Eastern France, Tectonophysics, 778, 228178, https://doi.org/10.1016/j.tecto.2019.228178, 2020.

Sternai, P., Sue, C., Husson, L., Serpelloni, E., Becker, T. W., Willett, S. D., Faccenna, C., Di Giulio, A., Spada, G., Jolivet, L., Valla, P., Petit, C., Nocquet, J.-M., Walpersdorf, A., and Castelltort, S.: Present-day uplift of the European Alps: Evaluating mechanisms and models of their relative contributions, Earth-Sci. Rev., 190, 589–604, https://doi.org/10.1016/j.earscirev.2019.01.005, 2019.

Sue, C. and Tricart, P.: Late Alpine brittle extension above the Frontal Pennine Thrust near Briançon, Western Alps, Eclogae Geol. Helv., 92, 171–181, https://doi.org/10.5169/SEALS-168659, 1999.

Sue, C. and Tricart, P.: Neogene to ongoing normal faulting in the inner western Alps: a major evolution of the alpine tectonics, Tectonics, 22, 1–25, https://doi.org/10.1029/2002TC001426, 2003.

Sue, C., Thouvenot, F., Fréchet, J., and Tricart, P.: Widespread extension in the core of the western Alps revealed by earthquake analysis, J. Geophy. Res.-Sol. Ea., 104, 25611–25622, https://doi.org/10.1029/1999JB900249, 1999.

Sue, C., Delacou, B., Champagnac, J.-D., Allanic, C., Tricart, P., and Burkhard, M.: Extensional neotectonics around the bend of the Western/Central Alps: an overview, Int. J. Earth Sci. (Geol Rundsch), 96, 1101–1129, https://doi.org/10.1007/s00531-007-0181-3, 2007.

Tardy, M., Deville, E., Fudral, S. E. R. E., Guellec, S., Ménard, G., Thouvenot, F., and Vialon, P.: Interprétation structurale des données du profil de sismique réflexion profonde ECORS-CROP Alpes entre le front Pennique et la ligne du Canavese (Alpes occidentales), Mém. S. Géo. F., 156, 217–226, 1990.

Thouvenot, F., Fréchet, J., Pinter, N., Gyula, G., Weber, J., Stein, S., and Medak, D. (Eds.): Seismicity along the northwestern edge of the Adria Microplate, The Adria Microplate: GPS Geodesy, Tectonics and Hazards, Nato Si. S. IV Ear. En. Kluwer Academic Publishers, Dordrecht, the Netherlands, 335–349, https://doi.org/10.1007/1-4020-4235-3_23, 2006.

Tricart, P.: From passive margin to continental collision; a tectonic scenario for the Western Alps, Am. J. Sci., 284, 97–120, https://doi.org/10.2475/ajs.284.2.97, 1984.

Tricart, P., Schwartz, S., Sue, C., Poupeau, G., and Lardeaux, J.-M.: La denudation tectonique de la zone ultradauphinoise et l'inversion du front brianconnais au sud-est du Pelvoux (Alpes occidentales); une dynamique miocene a actuelle, B. Soc. Geol. Fr., 172, 49–58, https://doi.org/10.2113/172.1.49, 2001.

Tricart, P., Lardeaux, J.-M., Schwartz, S., and Sue, C.: The late extension in the inner western Alps: a synthesis along the south-Pelvoux transect, B. Soc. Geol. Fr., 177, 299–310, https://doi.org/10.2113/gssgfbull.177.6.299, 2006.

Tricart, P., Van Der Beek, P., Schwartz, S., and Labrin, E.: Diachronous late-stage exhumation across the western Alpine arc: constraints from apatite fission-track thermochronology between the Pelvoux and Dora-Maira Massifs, J. Geol. Soc., 164, 163–174, https://doi.org/10.1144/0016-76492005-174, 2007.

Vermeesch, P.: IsoplotR: A free and open toolbox for geochronology, Geosci. Front., 9, 1479–1493, https://doi.org/10.1016/j.gsf.2018.04.001, 2018.

Walker, J., Cliff, R. A., and Latham, A. G.: U-Pb isotopic age of the StW 573 hominid from Sterkfontein, South Africa, Science, 314, 1592–1594, https://doi.org/10.1126/science.1132916, 2006.

Walpersdorf, A., Pinget, L., Vernant, P., Sue, C., Deprez, A., and the RENAG team: Does Long-Term GPS in the Western Alps Finally Confirm Earthquake Mechanisms?, Tectonics, 37, 3721–3737, https://doi.org/10.1029/2018TC005054, 2018.

Wells, D. L. and Coppersmith, K. J.: New empirical relationships among magnitude, rupture length, rupture width, rupture area, and surface displacement, B. Seismol. Soc. Am., 84, 974–1002, 1994.

Woodhead, J. D. and Hergt, J. M.: Strontium, Neodymium and Lead Isotope Analyses of NIST Glass Certified Reference Materials: SRM 610, 612, 614, Geostand. Geoanal. Res., 25, 261–266, https://doi.org/10.1111/j.1751-908X.2001.tb00601.x, 2001.

Zhao, L., Paul, A., Solarino, S., Guillot, S., Malusà, M., Zheng, T., Aubert, C., Salimbeni, S., Dumont, T., Schwartz, S., Pondrelli, S., Zhu, R., and Wang, Q.: First seismic evidence for continental subduction beneath the Western Alps, Geology, 43, 815–818, https://doi.org/10.1130/G36833.1, 2015.